ChemComm

Check for updates

Reversible P–P bond cleavage at an iridium(III) metal centre†

Simon J. Coles, [a] Peter N. Horton, [a] Patrick Kimber, [b] Wim T. Klooster, [a] Pingchuan Liu, [b] Felix Plasser, [b] Martin B. Smith [*b] and Graham J. Tizzard [a]

Treatment of a κ^1-P-monodentate bicyclic diphosphane iridium(III) complex with a labile gold(I) precursor afforded an unusual Ir^{III}/Au^I complex in which the P–P single bond has been cleaved. This reaction was cleanly reversed upon addition of tertiary phosphine. Carbon–carbon bond activation, across neighbouring P_2C_2N rings of the coordinated bicyclic diphosphane, occurred upon thermolysis of the Ir^{III}/Au^I complex.

Phosphorus based compounds underpin many significant advances that have been achieved in the fields of synthesis, reactivity and mechanistic understanding, and in catalysis. In this context, the ubiquitous tertiary phosphines stand out as excellent examples of highly tuneable ligands for various transition metals. By contrast, the coordination chemistry of P-based compounds such as terminal/bridging phosphides (PR_2^-)[1] and, to a lesser extent, diphosphanes (R_2P-PR_2),[2] have witnessed relatively few studies. In spite of this, there is a growing interest[3] in new synthetic routes to R_2P-PR_2 compounds given also the importance of P–P bonded species in organophosphorus chemistry. Metal bound phosphide ligands can undergo P–P radical coupling leading to dimeric products,[4] in a few instances this process is reversible (Chart 1).[5] Furthermore, diphosphanes have been shown to undergo homolytic P–P bond cleavage affording $R_2P^\bullet$ radicals.[6] The reactivity of R_2P-PR_2 towards soft transition metals has been shown to result in rapid P–P bond cleavage and formation of terminal or bridging phosphido ligands (Chart 1). A terminal phosphido Rh^V intermediate has been implicated in the dehydrocoupling of HPR_2 affording R_2P-PR_2.[7] Tsipis and

co-workers also reported the reversible transformation of two bridging PPh_2^- ligands to a neutral, μ-Ph_2P-PPh_2 ligand at a trinuclear Pt_2Pd core.[8] Herein we describe the intramolecular P–P cleavage of a well-defined $Ir^{III}(\kappa^1$-$R_2P-PR_2)$ complex upon treatment with a labile gold(I) source and, moreover, shown this to be a reversible process. Under thermal conditions we also observed an unexpected C–C bond activation across both P_2C_2N rings of a coordinated bicyclic diphosphane.

Various groups[2,3,6,9–12] have reported the synthesis and reactivity of several types of R_2P-PR_2, with acyclic variants being most common. We reasoned a "rigid" R_2P-PR_2 would reduce P–P bond rotation/dissociation yet still function as a bridging ligand. Accordingly, the new air stable bicyclic diphosphane, **P–P(OMe)**, was readily synthesised in 44% yield by a one-step reaction between $[P(CH_2OH)_4]Cl$ and 4-$H_2NC_6H_4OMe$ (see ESI† for details).[13,14] The $^{31}P\{^1H\}$ NMR spectrum of a $CDCl_3$ solution of **P–P(OMe)** displayed a singlet at δ -34.7 ppm and the single crystal X-ray structure (Fig. 1) confirmed a bicyclic five-membered arrangement with a typical P–P bond length of $2.2042(7)$ Å.[12] The nitrogen atoms are nearly planar (sum of

a UK National Crystallography Service, School of Chemistry, University of Southampton, Southampton, SO17 1BJ, UK
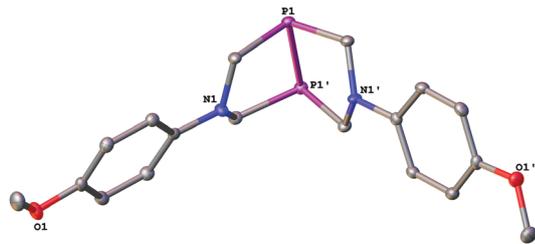
b Department of Chemistry, Loughborough University, Loughborough, Leics, LE11 3TU, UK. E-mail: m.b.smith@lboro.ac.uk
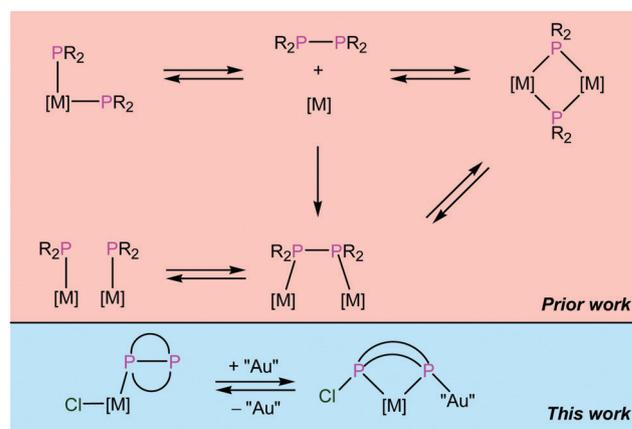
Chart 1 Interplay between PR_2^- and R_2P-PR_2 (R = alkyl, aryl) metal chemistry *via* oxidative P–P coupling/cleavage reactions.
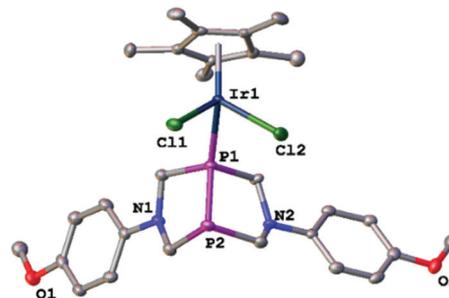
Fig. 1 Molecular structure of **P–P(OMe)** in the solid state. Thermal ellipsoids are drawn at the 50% probability level. All hydrogen atoms have been omitted for clarity. Selected bond length [Å]: P(1)–P(1′) 2.2042(7) Å. Symmetry operator: $1 - x$, $1 y$, $+z$.

Fig. 2 Molecular structure of **1** in the solid state. Thermal ellipsoids drawn are at the 50% probability level. All hydrogen atoms have been omitted for clarity. Selected bond lengths [Å] and angles [°]: Ir(1)–P(1) 2.2705(13), Ir(1)–Cl(1) 2.4034(13), Ir(1)–Cl(2) 2.4155(15), P(1)–P(2) 2.1836(19); Cl(1)–Ir(1)–P(1) 89.25(5), Cl(2)–Ir(1)–P(1) 82.33(5), Cl(1)–Ir(1)–Cl(2) 89.49(5).

angles approx. 350°) whilst the C(1)–P(1)–P(1′)–C(1′) torsion angle between both five-membered rings is 118.65(6)°. Conformational restriction imposed by the two adjacent, five-membered, P_2C_2N rings dictates the orientation of the two phosphorus lone pairs are *syn* disposed.

Reaction of 2 equiv. of **P–P(OMe)** and $[IrCl(\mu-Cl)(\eta^5-C_5Me_5)]_2$ in CH_2Cl_2 gave **1** in excellent yield (88%) as a yellow solid (Scheme 1). The $^{31}P\{^1H\}$ NMR spectrum showed the expected AX spectrum consistent with κ^1-mode (Ir^{III}–P$_{coord}$, δ 15.8 ppm; P$_{free}$, δ −56.3 ppm, J_{PP} = 230 Hz) and was further supported by the appearance of two ^{13}C signals for the methylene carbon atoms (δ 54.5 ppm, J_{PC} = 28 Hz; δ 52.1 ppm, J_{PC} = 24 Hz). Reaction of 1 equiv. of **P–P(OMe)** and $[IrCl(\mu-Cl)(\eta^5-C_5Me_5)]_2$ in CH_2Cl_2 gave the dinuclear Ir^{III} complex **1′** which showed a singlet at δ −7.2 ppm consistent with a highly symmetric bridged structure and two P-bound $\{IrCl_2(\eta^5-C_5Me_5)\}$ groups. The X-ray structure of **1** (Fig. 2) shows a slightly contracted P–P bond length of 2.1836(19) Å, with respect to **P–P(OMe)**, whilst the nitrogen atoms in **1** are nearly planar [sum of angles 351° around N(1); 345° around N(2)].

Given the available free P-coordination site in **1** we sought to explore whether a second, different, soft metal centre could be supported on a R_2P-PR_2 ligand. Hence, reaction of **1** with AuCl(tht) (tht = tetrahydrothiophene) in CH_2Cl_2 at r.t. gave, instead, compound **2** in excellent yield (83%) as a pale yellow solid. The ^{31}P NMR spectrum of **2** showed an AX pattern, with a significantly reduced J_{PP} coupling of 53.4 Hz, consistent with two distinct, non-bonded, P centres and further supported by the ^1H NMR spectrum which showed two sets of aromatic resonances consistent with non-equivalent –C_6H_4OMe rings.

The most significant feature of the X-ray structure of **2** (Fig. 3) is insertion[15] of an "Ir($\eta^5-C_5Me_5$)Cl" fragment, coupled with P–P bond cleavage [P···P interatom separation is 2.8839(18)/2.8941(18) Å] and migration of Cl to P(1)[16] and a terminal AuCl group on P(2). The nitrogen atoms are significantly more distorted (sum of angles 340–346°) and there is a strong aurophilic Au···Au interaction [2.9278(3) Å] between neighbouring molecules.[17] The bond lengths for Ir(1)–P(2)/P(2)–Au(2)/Au(1)–Cl(3) are similar to reported
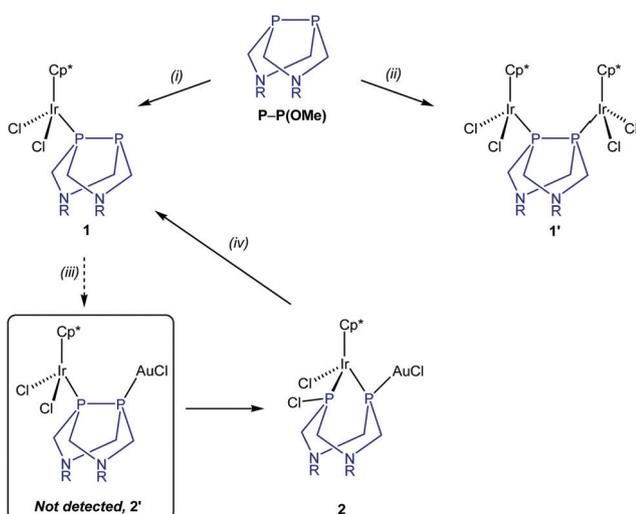
Scheme 1 Synthesis of **P–P(OMe)**, **1**, **1′** and **2**. Reaction conditions: (i) 2 equiv. **P–P(OMe)**/[IrCl(μ-Cl)($\eta^5-C_5Me_5$)] (ii) 1 equiv. **P–P(OMe)**/ [IrCl(μ-Cl)($\eta^5-C_5Me_5$)] (iii) AuCl(tht) (iv) 1 equiv. PPh₃, − AuCl(PPh₃). R = 4-C_6H_4OMe; Cp* = $\eta^5-C_5Me_5$.
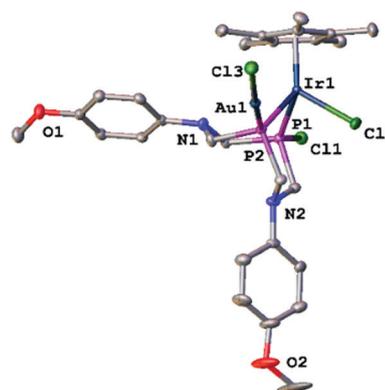
Fig. 3 Molecular structure of **2·CDCl₃** in the solid state. Thermal ellipsoids are drawn at the 50% probability level. All hydrogen atoms and solvent have been omitted for clarity. Selected bond lengths [Å] and angles [°] (values in parentheses are for the second independent molecule): Ir(1)–P(1) 2.2111(13) [2.2095(14)], Ir(1)–Cl(2) 2.3965(12) [2.3967(13)], Ir(1)–P(2) 2.3318(13) [2.3381(13)], Au(1)–P(2) 2.2429(12) [2.2525(13)]; Cl(3)–Au(1) 2.3252(12) [2.3273(13)], P(1)–Cl(1) 2.0389(17) [2.0510(18)]; P(1)–Ir(1)–P(2) 78.76(5) [78.99(5)], Cl(2)–Ir(1)–P(1) 92.21(5) [95.04(5)], Cl(2)–Ir(1)–P(2) 88.83(5) [87.70(5)], Cl(3)–Au(1)–P(2) 172.32(5) [174.09(5)].

examples[18,19] whilst the Ir(1)–P(1)/Ir(1)–P(2) bond distances differ reflecting the bonding arrangements of both phosphorus donors [P(2) bridges both Au[I] and Ir[III] centres].

In order to gain more insight into the reaction pathway leading to **2** from **1** via **2′**, we undertook density functional theory calculations (see ESI† for details). An accessible transition state between **2′** and **2** (TS, 18.6 kcal mol^{-1}), following initial migration of a chlorine atom to P(1), with the P–P bond intact was located and optimised (Fig. 4). The formation of **2** from **2′** is exothermic by -3.5 kcal mol^{-1}. It is unlikely steric factors are solely important here given that **P–P(OMe)** can accommodate two, bulky, {IrCl(η^5-C$_5$Me$_5$)} groups (as in **1′**) across the P–P single bond vector suggesting electronic effects contribute. Natural bond orbital (NBO) analysis for **2** (see ESI† for details) confirmed a near perfect sp^3 hybridisation of P(2) as a phosphido with a dative bond to AuCl. Conversely, in **2′** enhanced p orbital character is associated to the P–P single bond, leaving the P(2) lone pair sp hybridised and unable to form a strong Au–P bond.

When **2** was treated with 1 equiv. of PPh$_3$, in CDCl$_3$, clean conversion to **1** occurred (as monitored by in situ ^{31}P{^{1}H} NMR, Fig. 5), accompanied by concomitant formation of AuCl(PPh$_3$) (δ 33.8 ppm). No reaction took place between **1** and AuCl(PPh$_3$) acting as the source of "AuCl".

Whilst complex **1** shows good thermal stability (C$_7$H$_8$, reflux, 24 h), heating a CDCl$_3$ solution of **2** for 4 d at ca. 50 °C did not result in any observable formation of **1**. Instead, in situ monitoring by ^{31}P{^{1}H} NMR (Scheme 2) revealed the appearance of a new AX pattern (δ 50.5 ppm, -30.2 ppm, J_{PP} = 55.2 Hz), along with a second minor species and significant amounts of decomposition products. The ^{1}H NMR spectrum of **3**, after fractional crystallisation ($\sim$20% isolated yield) from CDCl$_3$ solution, showed seven unique aliphatic hydrogens suggesting formation of a new C–C bond across neighbouring P$_2$C$_2$N rings. The X-ray structure of **3** (Fig. 6) again confirmed the absence of a P–P bond [P···P separation 2.943(3) Å] and on P(1) a chlorine atom and P(2) a terminal AuCl group. The nitrogen atoms are significantly more distorted [sum of angles 343° around N(1); 346° around N(2)]. Most significantly a new C–C single bond
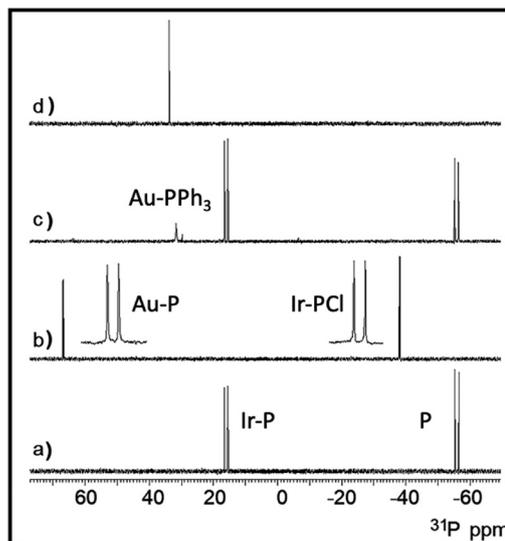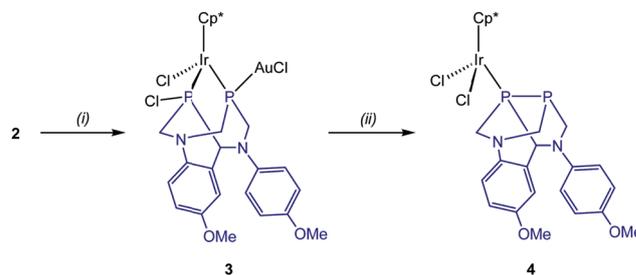

Fig. 5 ^{31}P{^{1}H} NMR spectra of (a) complex **1** (b) complex **2** (c) in situ addition of 1 equiv. PPh$_3$ to **2** (d) AuCl(PPh$_3$).

Scheme 2 Thermal conversion of **2** to **3** and reversible P–P coupling to generate **4** as a pair of diastereomers. Reaction conditions: (i) heat, CDCl$_3$ (ii) 1 equiv. PPh$_3$, − AuCl(PPh$_3$). Cp* = η^5-C$_5$Me$_5$.
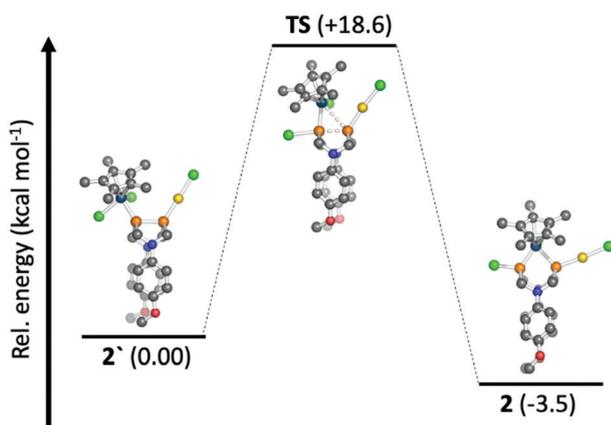

Fig. 4 Energy profile (kcal mol^{-1}) for the P–P cleavage of **2**.
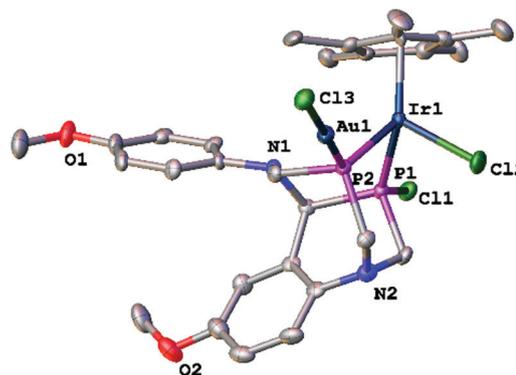

Fig. 6 Molecular structure of **3**·CDCl$_3$ in the solid state. Thermal ellipsoids are drawn at the 50% probability level. All hydrogen atoms and solvent have been omitted for clarity. Selected bond lengths [Å] and angles [°]: Ir(1)–P(1) 2.233(2), Ir(1)–Cl(2) 2.403(2), Ir(1)–P(2) 2.328(2), Au(1)–P(2) 2.245(2), Au(1)–Cl(3) 2.302(2) P(1)–Cl(1) 2.063(3); P(1)–Ir(1)–P(2) 80.34(8), Cl(2)–Ir(1)–P(1) 91.32(8), Cl(2)–Ir(1)–P(2) 90.75(8), Cl(3)–Au(1)–P(2) 177.60(8).

[1.511(11) Å] leads to a unusual bicyclic ligand framework. The closest Au···Au interaction between neighbouring molecules is approx. 10 Å, significantly different form that observed for **2**. Treatment of **3** with 1 equiv. of PPh₃ afforded cleanly **4**, as two diastereomers (*ca.* 50:50), as shown by their diagnostic AX patterns (*in situ* $^{31}P\{^{1}H\}$ NMR studies, see ESI† for details).

In conclusion, this study highlights the reversible, intra-molecular insertion of a late transition metal entity across a P–P single bond of a coordinated diphosphane. By virtue of flexible, neighbouring arene substituents on the diphosphane, we observed an unprecedented C_{sp2}–C_{sp3} coupling affording a highly functionalised P-ligand. Further studies will be directed towards exploring the ligand scope, reactivity and P–P/C–C mechanistic aspects of these transformations.

Conflicts of interest

There are no conflicts of interest to declare.

Notes and references

1 (*a*) C. Fortuño, A. Martin, P. Mastrorilli, M. Latronico, V. Petrelli and S. Todisco, *Dalton Trans.*, 2020, **49**, 4935–4955; (*b*) J. Yang, S. Langis-Barsetti, H. C. Parkin, R. McDonald and L. Rosenberg, *Organometallics*, 2019, **38**, 3257–3266; (*c*) K. Kaniewska, A. Dragulescu-Andrasi, L. Ponikiewski, J. Pikies, S. A. Stoian and R. Grubba, *Eur. J. Inorg. Chem.*, 2018, 4298–4308; (*d*) U. Fischbach, M. Trincado and H. Grützmacher, *Dalton Trans.*, 2017, **46**, 3443–3448.
2 (*a*) S. Molitor, C. Mahler and V. H. Gessner, *New J. Chem.*, 2016, **40**, 6467–6474; (*b*) D. Tofan and C. C. Cummins, *Chem. Sci.*, 2012, **3**, 2474–2478.
3 For a recent example, see: I. Elser, R. J. Andrews and D. W. Stephan, *Chem. Commun.*, 2022, **58**, 1740–1743.
4 M. W. Bezpalko, B. M. Foxman and C. M. Thomas, *Inorg. Chem.*, 2013, **52**, 12329–12331.
5 (*a*) S. Kim and Y. Lee, *Inorg. Chem. Front.*, 2020, **7**, 1172–1181; (*b*) Y.-E. Kin and Y. Lee, *Angew. Chem., Int. Ed.*, 2018, **57**, 14159–14163; (*c*) A. Tohmé, G. Grelaud, G. Argouarch, T. Roisnel, S. Labouille, D. Carmichael and F. Paul, *Angew. Chem., Int. Ed.*, 2013, **52**, 4445–4448.
6 (*a*) C. Branfoot, T. A. Young, D. F. Wass and P. G. Pringle, *Dalton Trans.*, 2021, **50**, 7094–7104; (*b*) M. Blum, O. Puntigam, S. Plebst, F. Ehret, J. Bender, M. Nieger and D. Gudat, *Dalton Trans.*, 2016, **45**, 1987–1997; (*c*) J.-D. Guo, S. Nagase and P. P. Power, *Organometallics*, 2015, **34**, 2028–2033; (*d*) N. A. Griffin, A. D. Hendsbee, T. L. Roemmele, M. D. Lumsden, C. C. Pye and J. D. Masuda, *Inorg. Chem.*, 2012, **51**, 11837–11850.
7 V. P. W. Böhm and M. Brookhart, *Angew. Chem., Int. Ed.*, 2001, **40**, 4694–4696.
8 J. Forniés, C. Fortuño, S. Ibáñez, A. Martín, A. C. Tsipis and C. A. Tsipis, *Angew. Chem., Int. Ed.*, 2005, **44**, 2407–2410.
9 S. Molitor, J. Becker and V. H. Gessner, *J. Am. Chem. Soc.*, 2014, **136**, 15517–15520.
10 D. M. C. Ould, T. T. P. Tran, J. M. Rawson and R. L. Melen, *Dalton Trans.*, 2019, **48**, 16922–16935.
11 A. K. King, A. Buchard, M. F. Mahon and R. L. Webster, *Chem. – Eur. J.*, 2015, **21**, 15960–15963.
12 N. Szynkiewicz, L. Ponikiewski and R. Grubba, *Dalton Trans.*, 2018, **47**, 16885–16894.
13 A. W. Frank and G. L. Drake, Jr., *J. Org. Chem.*, 1977, **42**, 4125–4127. We have shown, by ^{31}P NMR studies, that this reaction proceeds via the intermediate $P\{CH_2N(H)C_6H_4OMe\}_3$ and we also observe the phosphine oxide. Due to the low solubility of **P-P(OMe)** in methanol, this compound readily separates from other methanol soluble P-based compounds. This reaction has previously been observed only for $C_6H_5NH_2$ (see ref. 14).
14 A. W. Frank and G. L. Drake, Jr., *J. Org. Chem.*, 1972, **37**, 2752–2755.
15 R. Franz, S. Nasemann, C. Bruhn, Z. Kelemen and R. Pietschnig, *Chem. – Eur. J.*, 2021, **27**, 641–648.
16 M. J. Ray, M. Bühl, L. J. Taylor, K. S. Athukorala Arachchige, A. M. Z. Slawin and P. Kilian, *Inorg. Chem.*, 2014, **53**, 8538–8547.
17 P. Pyykko, *Chem. Soc. Rev.*, 2008, **37**, 1967–1997.
18 Y. Gloaguen, W. Jacobs, B. de Bruin, M. Lutz and J. I. van der Vlugt, *Inorg. Chem.*, 2013, **52**, 1682–1684.
19 M. Brym, C. Jones and J. D. E. T. Wilton-Ely, *Inorg. Chem.*, 2005, **44**, 3275–3282.